Measurement and model analysis of (n,xα) cross sections for Cr, Fe, ^{59}Co, and ^{58,60}Ni from threshold energy to 150 MeV

S. Kunieda, R. C. Haight, T. Kawano, M. B. Chadwick, S. M. Sterbenz, F. B. Bateman, O. A. Wasson, S. M. Grimes, P. Maier-Komor, H. Vonach, T. Fukahori, and Y. Watanabe

Phys. Rev. C **85**, 054602 — Published 1 May 2012

DOI: 10.1103/PhysRevC.85.054602

Measurement and Model Analysis of $(n, x\alpha)$ Cross Sections for Cr, Fe, ^{59}Co and ^{58,60}Ni from Threshold Energy to 150 MeV

S. Kunieda*
Los Alamos National Laboratory, Los Alamos, New Mexico 87545 and
Nuclear Data Center, Japan Atomic Energy Agency, Tokai-mura Naka-gun, Ibaraki 319-1195, Japan

R. C. Haight, T. Kawano, M. B. Chadwick, and S. M. Sterbenz
Los Alamos National Laboratory, Los Alamos, New Mexico 87545

F. B. Bateman and O. A. Wasson
National Institute of Standards and Technology, Gaithersburg, Maryland 20899

S. M. Grimes
Institute of Nuclear and Particle Physics, Department of Physics and Astronomy, Ohio University, Athens, Ohio 45701

P. Maier-Komor
Physik-Department, Technische Universität München, James-Franck-Str., D-85748 Garching, Germany

H. Vonach
Institut für Radiumforschung und Kernphysik der Universität Wien, Boltzmanngasse 3, 1090 Wien, Austria

T. Fukahori
Nuclear Data Center, Japan Atomic Energy Agency, Tokai-mura Naka-gun, Ibaraki 319-1195, Japan

Y. Watanabe
Department of Advanced Energy Engineering Science,
Kyushu University, Kasuga, Fukuoka, 816-8580, Japan
(Dated: March 30, 2012)

Neutron reactions that produce alpha-particles have been investigated experimentally and analyzed by reaction model calculations for incident neutron energies from threshold to 150 MeV on elemental chromium and iron. The cross sections were measured at the Los Alamos Neutron Science Center by direct observation of alpha-particles. Previous data on isotopes ^{59}Co and ^{58,60}Ni were also included in the analysis. The model calculations are made for both statistical decay and pre-equilibrium processes. This study particularly focuses on the pre-equilibrium cluster emission, which is described by the clustering exciton model of Iwamoto and Harada. We calculate the alpha-particle formation factors numerically without any approximations that appeared in the original model. The model parameter ΔR, the nuclear surface area where the pickup reaction may occur, is determined by fitting the calculated alpha-particle energy spectra to experimental data. The calculated alpha-particle production cross sections agree well with the measured data, except for the Cr case. With a simple sensitivity study for the level density parameters, it is reported that relatively small changes in the level density parameters improve reproduction of experimental data significantly. Our realistic model calculations for the pre-equilibrium process shed light on uncertainties in the nuclear level densities in the statistical decay calculation.

PACS numbers:

I. INTRODUCTION

A long-standing problem exists in the model prediction of composite-particle production cross sections in nucleon induced nuclear reactions. We can partially ascribe this problem to the pre-equilibrium model calculation where our knowledge of the composite particle emission is limited. The phenomenological models proposed by Kalbach [1, 2] describe a nucleon-transfer reaction process accounting for phase-space, in which many adjustable parameters are involved to fit experimental particle energy spectra. Although a global parameterization is reported [1, 3], extrapolation of the global parameters beyond the experimental range requires caution. The alpha-particle exhibits a typical clustering nature where four nucleons are tightly bound. The clustering exciton model proposed by Iwamoto and Harada [4] simulates the pickup process by nucleons, where both bound and unbound nucleons are involved in the reaction. The

*kunieda.satoshi@jaea.go.jp;

Iwamoto-Harada model calculates the overlap integral of wave functions for the alpha-particle and four nucleons near the nuclear surface in the phase-space, and consequently it yields the alpha-particle formation factor that is used for calculating the alpha-particle emission probabilities in the exciton model [2]. The original calculation made by Iwamoto and Harada employed a root-mean-square (rms) approximation [4] where no correlations existed between the coordinates in the phase-space, which consequently leads to a systematically larger nuclear surface region [4, 5] as will be shown in this paper. Zhang *et al.* first performed the exact calculation of the formation factors [6]. They reported an explicit and useful computational approach for the multiple phase-space integration of the wave functions. However, they did not impose the radial condition that defines the surface region where the pickup process occurs. In addition, there were no discussions on the difference between the approximated and exact calculations. The difference might be compensated by modifications of the adopted model parameters, a possibility which will be discussed in this paper.

The purpose of this study is to advance the clustering exciton model calculation for the alpha-particle emission. The applicability of the pre-equilibrium model is investigated through comparisons with our experimental $(n, x\alpha)$ cross sections for chromium, iron and isotopes ^{59}Co and ^{58,60}Ni. Alpha-particle emission takes place in both the compound reaction and the pre-equilibrium processes, which are clearly separated by the reaction time-scale. The fraction of the pre-equilibrium emission, as we discuss in this paper, is important for determining the energy spectra of the emitted alpha-particles, and also constrains the prediction of the total alpha-particle production cross sections. This study is also motivated by an application in nuclear technology. It is known that the radiation damage of materials is strongly related to the accumulation of helium gas produced by the $(n, x\alpha)$ reaction. There are (will be) nuclear applications that involve high neutron (or proton) fluences such as in nuclear fission reactors and, in the future, fusion reactors and also at accelerator-based facilities. Therefore, it is important to evaluate alpha-particle production cross sections in order to understand mechanical properties of material under irradiation conditions. The target nuclei we chose are important as structural elements in those nuclear applications.

The calculation is based on the Hauser-Feshbach code GNASH [7]. The exciton model [2] is incorporated into the code to calculate the pre-equilibrium process. When an incident nucleon energy is so high that more than one exciton is in the continuum, multi-particle pre-equilibrium emissions [8] occur. These models tend to predict the energy spectra of secondary nucleons and total nucleon production cross sections fairly well, as they are frequently used in the nuclear data evaluations [9]. For the pre-equilibrium composite-particle emissions, GNASH employs the model of Kalbach [2]. In this work, instead the clustering model of Iwamoto-Harada is incorporated into GNASH to calculate pre-equilibrium alpha-particle emission. We perform the clustering calculations without the rms approximation, where we impose the surface condition to the phase-space integration. We optimize the pre-equilibrium and the clustering model parameters simultaneously by comparing with experimental proton and alpha-particle energy spectra, and obtain a local but unique parameter set in the mass region we are interested in.

Experimental $(n, x\alpha)$ data exist for several reactions on the target nuclei of this report. Because we are concentrating on incident neutron energies above 14 MeV, we will show comparisons of calculations with data in this region that come from three laboratories. The complete alpha-particle production cross sections, including the evaporation alphas at low energy, were measured for a wide range of incident neutron energies with the spallation neutron source at Los Alamos Neutron Science Center (LANSCE). These data cover the energy range from the threshold to 50 MeV for ^{59}Co and ^{58,60}Ni, and to 100 MeV for elemental Cr and Fe, where the pickup mechanism is dominant. The data for ^{59}Co have been published with experimental details previously [10] and a preliminary was made for the nickel isotopes [11, 12]. The cross sections for Cr and Fe were newly measured by following the same experimental technique (though preliminary data have reported elsewhere [13]). There is good agreement of these data with the many measurements made with a variety of techniques and reported in the literature at 14 MeV, and with a smaller number of measurements at lower energies. In this paper, we first give a summary of those our LANSCE experiment. At other laboratories, partial alpha-particle spectra that concentrate on the pre-equilibrium part of the spectra were measured in detail at principally at 62.7 MeV, and with larger statistical errors, at energies from 25 to 53 MeV on iron and cobalt [14]. Also a detailed monoenergetic measurement on iron was made at 96 MeV [15].

The present work is part of a research study conducted by numerous groups over the years to better understand higher energy neutron-induced charged particle production, with the goal of advancing our knowledge of the nuclear reaction mechanisms and the nuclear level densities involved, and providing evaluated data for applications. In addition to the aforementioned applications in gas production and material damage, other applications include neutron heating (kerma) for radiation therapy [16, 17] and single-event upsets [18, 19].

II. EXPERIMENTAL SUMMARY

The experimental approach for the new data reported here has been described previously for measurements on ^{59}Co [10]. The experiments were carried out at the Weapons Neutron Research (WNR) facility of LANSCE where neutrons are produced by spallation reactions of

the bunched 800-MeV proton beam on a tungsten target. The neutrons produced at 90-degrees were collimated and then were incident on samples of elemental chromium, iron and isotopically enriched samples ^{58}Ni and ^{60}Ni. For Fe, the detection apparatus was moved to a 15-degree flight path to enhance the flux of high energy neutrons.

The targets used were self-supporting metal foils approximately 10 cm in diameter with thicknesses as follows: ^{nat}Cr(18.8 and 36.5 mg/cm^2), ^{nat}Fe (6 thicknesses from 2.36 to 39.5 mg/cm^2, 99%), ^{58}Ni (3.38 mg/cm^2, 99.66%) and ^{60}Ni (2.98 mg/cm^2, 99.79%). The thinner chromium sample was thick enough to stop the lowest energy alpha-particles that would have transited the full thickness, and so a correction was made for these unobserved alpha-particles. Alpha-particles produced on possible contaminants such as oxygen and carbon were not observed on any of the samples.

Charged particles resulting from neutron-induced reactions were detected by 4 counter telescopes each consisting of a proportional counter, a 500-micron silicon surface barrier detector, and a CsI(Tl) scintillator. With conventional ΔE-E data acquisition, the alpha-particles were identified. The telescopes were placed at 30, 60, 90 and 135 degrees relative to the direction of the incident neutron beam. For measurements of alpha-particle production in this energy range, nearly all of the alpha-particles stopped in the silicon detectors, which were thick enough to stop 33 MeV alphas. Alpha-particles with greater energy penetrated the silicon, but had low energy afterwards and therefore were not detected reliably in the CsI(Tl) detectors. These penetrating alpha-particles could be identified by their signals in the proportional counter and the silicon detector. Therefore, although the alpha-particle spectra were not measured well for alphas over 33 MeV, the number of alphas could be measured reliably for the full spectrum, even if it extended beyond 33 MeV. Low energy alpha-particles were measured well with the thin samples and the good performance of the low-pressure gas proportional counters. This latter capability differentiates these measurements from those of other laboratories as reported in the literature [14, 15, 20] for the measurement of the total alpha-particle production. As this report focuses on pre-equilibrium reactions, the spectra measured below 15-MeV incident neutron energy will be discussed in terms of the statistical nuclear reaction model in a subsequent publication [21].

Alpha-particle emission spectra were measured and then integrated over both emission energy and angle to produce the total alpha-particle production cross sections. Because the detectors obtained data at only 4 angles, and because the angular distribution of the alpha-particles, a systematic uncertainty of 15% was included in the angle-integrated cross sections.

III. THEORETICAL APPROACH

A. Computational Framework

1. Alpha-particle Formation Factors

The idea of a clustering model for pre-equilibrium emission was originally proposed by Iwamoto and Harada [4]. In this model, alpha-particle formation factors are calculated from the overlap integral between the wave functions of alpha-particle and four nucleons. It is symbolically expressed as $\langle\varphi_\alpha\chi^{(\epsilon_\alpha)}(\boldsymbol{R})|\phi_1\phi_2\phi_3\phi_4\rangle$ where φ_α and $\chi^{(\epsilon_\alpha)}(\boldsymbol{R})$ denote the intrinsic and the center-of-mass wave functions of alpha-particle, and $\phi_{1,\ldots,4}$ the wave functions of the single-particles. Numerically, the formation factor is calculated by the multiple integrations over the phase-space,

$$F_{l,m}(\epsilon_\alpha) = \frac{1}{(2\pi\hbar)^9}\int_S \prod_{i=1}^{3} d\boldsymbol{\xi_i} d\boldsymbol{p_{\xi_i}}, \tag{1}$$

where the coordinates $(\boldsymbol{\xi_i}, \boldsymbol{p_{\xi_i}})_{i=1,2,3}$ are introduced to describe relative motions of two N-N and one 2N-2N systems. The integration ranges are determined by the ground-state Hamiltonian of the alpha-particle under the conditions $p_{i=(1,\ldots,l)} \geq p_f$, $p_{j(=l+1,\ldots,4)} < p_f$ and $r_{i(=1,\ldots,4)} \leq R_{res} + \Delta R$, where p_f is the strength of Fermi momentum, R_{res} the radius of the residual nuclei. The symbol ΔR defines the nuclear surface where a pickup reaction may occur. This is a major parameter of this model, and determines the overall behavior of the formation factors that meet the condition

$$\sum_{l+m=4} F_{l,m}(\epsilon_\alpha) \leq 1. \tag{2}$$

In this study, the formation factors are calculated exactly by a numerical multiple integration. We follow the computational approach of Zhang *et al.* [6] but impose the condition of $r_{i(=1,\ldots,4)} \leq R_{res} + \Delta R$. The original calculation [4] had been performed under the rms approximation where no correlations existed between the coordinates in the phase-space. The differences between those two calculations (with/without the approximation) are illustrated for $F_{1,3}$, $F_{2,2}$, $F_{3,1}$ and $F_{4,0}$ in Fig. 1 as a function of the emitted alpha-particle energy. Those calculations were made for ^{59}Co under the condition of $\Delta R = 1.0$ fm, which was assumed in the original work. The approximation and exact calculations exhibit the same behavior, but the absolute values are apparently different. One may also notice that the high-energy tail lingers in the exact calculation, while it suddenly drops to zero at rather lower energies in the approximate calculation. In our data analysis, we consistently use the exact calculations of Eq. (1), which avoids any deficiencies coming from the rms approximation as shown in Fig. 1.

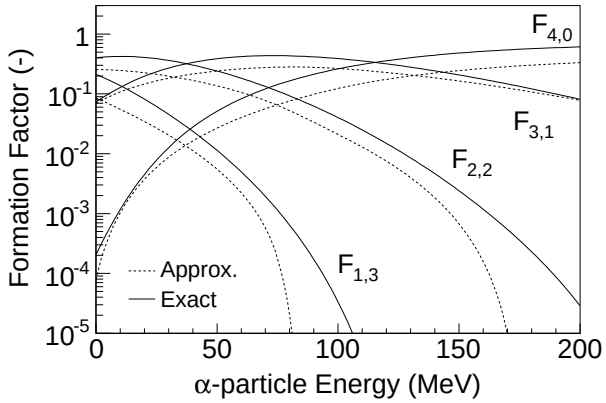

FIG. 1: The formation factors of alpha-particle $F_{l,m}$. The solid and dashed curves correspond to the calculations obtained by the exact integration and the rms approximation, respectively. Those calculations are for ^{59}Co under the condition of $\Delta R = 1.0$ fm, keeping the other parameters the same.

2. *Pre-equilibrium Model with Clustering*

In the exciton model, the angle-integrated particle emission cross sections are calculated by summing up the contributions from $n(= p + h)$ exciton states as

$$\frac{d\sigma}{d\epsilon} = \sigma_{cn} \sum_n W_x(n, \epsilon) P(n), \tag{3}$$

where the total reaction cross sections σ_{cn} is given by the optical model. The symbol $P(n)$ stands for the time-integrated occupation probability for the exciton stages. In GNASH, $P(n)$ is calculated with the closed form approximation [2]. The (p, h) pair creation rate $\lambda^+(p, h, E)$ is given by

$$\lambda^+(p, h, E) = \frac{2\pi}{\hbar} M^2 \frac{g^3 \{E - E_p(p+1, h+1)\}^2}{2(n+1)}, \tag{4}$$

where, $E_p(p, h) = [\max(p, h)]^2/g$ is Pauli energy, the parameters M^2 and g denote the average matrix element for two-body interaction and the inverse of the single-particle level spacing, respectively. The nucleon emission rates are calculated allowing those from the auxiliary $(p - h \neq 1)$ configurations [2]. Similarly, we compute the emission rate of alpha-particle by introducing the formation factor $F_{l,m}(\epsilon_\alpha)$ as

$$W_\alpha(p, h, \epsilon_\alpha) = \frac{1}{\pi^2 \hbar^3} \mu_\alpha \epsilon_\alpha \sigma_\alpha \frac{\displaystyle\sum_{l+m=4} F_{l,m}(\epsilon_\alpha) \left[\sum_{j=0}^{2} \omega(p-l, h-j, U) + \sum_{j=1}^{2} \omega(p-l-j, h, U) \right]}{\displaystyle\sum_{j=0}^{2} \omega(p, h-j, E) + \sum_{j=1}^{2} \omega(p-j, h, E)}, \tag{5}$$

where the symbol σ_α denotes the inverse reaction cross sections which is calculated from the optical model, and μ_α stands for the reduced mass. The single-particle state density $\omega(p, h, E)$ is given with the finite well depth correction [22, 23] as $\omega(p, h, E, \infty) f(p, h, E, V)$. The infinite expression is in Williams' form [24], and the finite correction factor is given by

$$f(p, h, E, V) = \sum_{i=0}^{h} (-1)^i \binom{h}{i} \left(\frac{E - iV}{E} \right)^{n-1} \Theta(E - iV). \tag{6}$$

The potential well depth V is set to 38 MeV, except for the initial stage where it is treated as a parameter due to the surface localization effect [25]. The code allows multiple particle emission in the pre-equilibrium stage with a simplified method [8]. In the present work, we also made it possible to calculate alpha-particle emission from the excited residual nuclei that were produced by the primary nucleon emission. It is given by introducing the formation factor as

$$\left(\frac{d\sigma}{d\epsilon_\alpha} \right)_{p,h} = \sum_{i=\pi,\nu} \int_{\epsilon_\alpha + B}^{U_{max}} \left(\frac{d\sigma}{dU} \right)_i T_\alpha(\epsilon_\alpha) \sum_{l+m=4} F_{l,m}(\epsilon_\alpha) \frac{g}{p} \frac{\omega(p-l, h, U - \epsilon_\alpha - B)}{\omega(p, h, U)} dU. \tag{7}$$

The excitation energy spectrum $d\sigma/dU$ is defined for the residual nuclei, which are produced by the primary neutron (π) or proton (ν) emission. The s-wave transmission coefficient $T_\alpha(\epsilon_\alpha)$ is calculated by using the Gamow factor [26].

B. Model Parameters

1. Optical Model Potential

The choice of optical model potential (OMP) is important in order to obtain reliable calculations. We employed a consistent coupled-channels local/global OMP [27] for both incoming and outgoing nucleons. The OMP covers the range of the present analysis as it is optimized in medium-to-heavy nuclei for induced nucleon energies up to 200 MeV. The optical model calculation is performed with the OPTMAN code [28] for nucleons, as in Ref. [27].

For outgoing alpha-particles, we adopted the recent version of the global OMP of Avrigeanu *et al* [29, 30]. Calculations are done using the ECIS code [31] assuming the spherical model. In general, the OMP of charged-particles are obtained above several tens of MeV where the experimental data of elastic-scattering cross sections are available. Avrigeanu *et al.* also validated their OMP in the low energy region by comparing the calculated (α, n), (α, p) and (α, γ) cross sections with available experimental data.

2. Level Density Parameters

It is important to assume physically reasonable level densities for all compound and residual nuclei in the Hauser-Feshbach calculation. The level density is calculated with the Gilbert and Cameron form [32], where the constant temperature model is used in the low excitation energy region, and the Fermi-gas model is used in the higher region. These two models are connected smoothly at a matching energy that is determined by the Fermi-gas parameter a and the experimental low-lying levels. The Fermi-gas parameter is calculated in the expression of Ignatyuk *et al.* [33],

$$a(U) = a^* \left\{ 1 + \Big[1 - \exp(\gamma U) \Big] \frac{\delta W}{U} \right\}, \qquad (8)$$

where the shell effect is considered by δW, which is washed out as the excitation energy U increases. The value of δW is obtained by subtracting the liquid-drop mass calculated by Myers and Swiatecki formula [34] from the experimental one. We keep the damping factor as the original work of Ignatyuk *et al.*, $\gamma = -0.054$, while the asymptotic level density parameter a^* is set to Arthur's systematics [7], $a^* = 0.1375A - 8.36 \times 10^{-5} A^2$ with a spin cutoff function $\sigma(U)^2 = 0.0888 A^{2/3} \sqrt{aU}$.

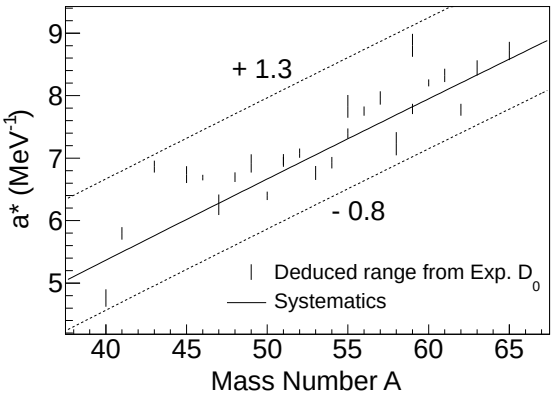

FIG. 2: Arthur's systematics for the asymptotic level density parameter a^* which is compared with the same values deduced from the experimental D_0 in the mass range A =40 – 65. The dashed lines represent our rough estimate of the uncertainty band.

Figure 2 shows a^* with the systematics and those deduced from the experimental D_0 values (the average resonance spacing for s-wave neutrons) that were taken from the latest compilation by Mughabghab [35] in the mass range A = 40 – 65. This systematics is reasonable as it reproduces average behavior of the experimental D_0 values. However, the experimental D_0 values scatter in the range +1.3 / −0.8 MeV^{-1}, which is shown by the dashed lines in the figure.

3. Pre-equilibrium Model Parameters

The average matrix element M^2 of Kalbach [36], which is defined as a function of the exciton energy and the composite mass, has a normalization constant K treated as an adjustable parameter. The effective potential well depth V is taken from the global pre-equilibrium analysis of Koning and Duijvestijn [3]. Although Kalbach's formulations [25, 37], include the V parameter, Koning and Duijvestijn obtained V for wider nuclear mass and energy ranges. The effective potential well depth gives a better reproduction of the high-energy end of experimental spectra. For the single-particle state density parameter, we adopted $g = 6a(U)/\pi^2$, where the symbol $a(U)$ is the energy dependent Fermi-gas level density parameter defined in Eq. (8).

The experimental (n, xp) pre-equilibrium spectra were reported by Nica *et al.* [38] for ^{59}Co at various incident energies from 25.5 to 62.7 MeV. Similar measurements were reported by Slypen *et al.* [20] for elemental Fe. The parameter K, the normalization constant for M^2, is determined so as to reproduce average behavior of those experimental data. It should be noted that

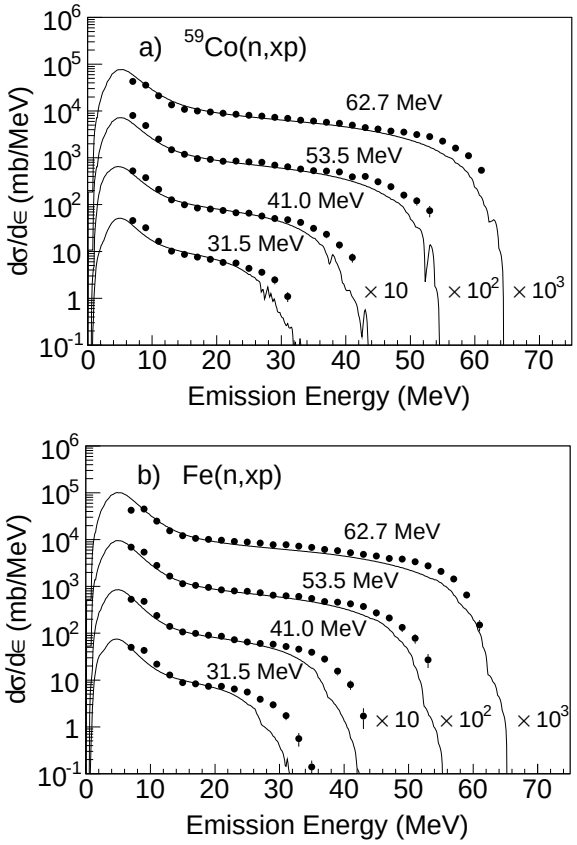

FIG. 3: Angle-integrated (n, xp) spectra for a) ^{59}Co and b) elemental Fe at incident energies of 31.5, 41.0, 53.5 and 62.7 MeV. The present calculations are compared with the experimental data of Nica *et al.* [38] for ^{59}Co and Slypen *et al.* [20] for Fe.

this parameter is totally independent of the clustering model parameters. According to this analysis, the value of $K = 180$ MeV^3 gives reasonable fits to the experimental data without any incident energy or target mass dependencies.

Figure 3 shows the calculated (n, xp) spectra for ^{59}Co and elemental Fe at the incident energies of 31.5, 41.0, 53.5 and 62.7 MeV. The calculated results reproduce measured data fairly well once M^2 is well determined. Taking the same pre-equilibrium parameters, similar agreements are achieved at all the incident energies. This is also confirmed by comparing with the experimental spectra of Fe(n, xp) at 96 MeV reported by Blideanu *et al.* [15]. One can see an underestimation at the high-end of spectra in Fig. 3. The reason is not so clear yet, but this is partly due to unknown experimental energy resolutions, as the data points sometimes exceed the reaction Q-value.

4. Clustering Model Parameters

We described the ground-state Hamiltonian of the alpha-particle by the harmonic-oscillator model in accordance with the original work of Iwamoto and Harada. The harmonic-oscillator parameter is chosen to give the rms of 1.6 fm, which is consistent with the experimental value. For the Fermi energy, we take 38 MeV irrespective of the nucleus. The radius of residual nuclei is set to $R_{res} = 1.5A^{1/3}$ fm as assumed in the original work.

The pickup radius ΔR is treated as an adjustable parameter since it substantially determines the absolute magnitude of spectra. This value is determined to give an overall description of experimental $(n, x\alpha)$ pre-equilibrium spectra, while keeping the other parameters untouched. We use the measured $(n, x\alpha)$ spectrum data of Nica *et al.* [38] for ^{59}Co and Slypen *et al.* [20] for elemental Fe. Although they were not able to discriminate helium-3 from the alpha-particle events in some cases, this is not a serious problem since $(n, x^3\mathrm{He})$ cross sections are very small in general. According to the present analysis, the value of ΔR is found to be 0.75 fm for both ^{59}Co and Fe, and no significant energy dependence is observed. We confirmed this by comparing our calculation with the experimental data of Fe$(n, x\alpha)$ at 96 MeV reported by Blideanu *et al.* [15]. In general, the pickup mechanism takes place in the vicinity of the nuclear surface, and the ΔR value obtained implies that the reaction likely occurs at a distance roughly half the size of an alpha-particle from the surface. Also, the value is similar to the nuclear diffuseness range where nucleons are loosely bound. Those findings support the physical picture of the reaction process as originally described by Iwamoto and Harada.

As examples, the calculated $(n, x\alpha)$ spectra are shown at 41.0 and 62.7 MeV in Fig. 4, together with the experimental data. In those calculated spectra, the largest contribution from the different configurations is of $(l, m) = (1, 3)$ at the $(p, h) = (2, 1)$ state. This situation is also illustrated in the original paper. The calculated spectrum reproduces measured data fairly well once ΔR is optimized. The use of $\Delta R = 1.0$ fm could be reasonable in the rms approximation. However, it overestimates the alpha-particle emission when the integration is performed exactly as shown in Fig. 4 (a). Therefore, the deficiency in the rms approximation is compensated by artificially increased ΔR values.

IV. COMPARISON BETWEEN MEASURED DATA AND CALCULATIONS

Our model calculations extend all the way up to 150 MeV, which is beyond the energy range of experimental data, to see the behavior of the calculations. The model parameters adopted are described in Sec. III B. Because we did not perform an individual optimization for each cross section, the calculations presented in this

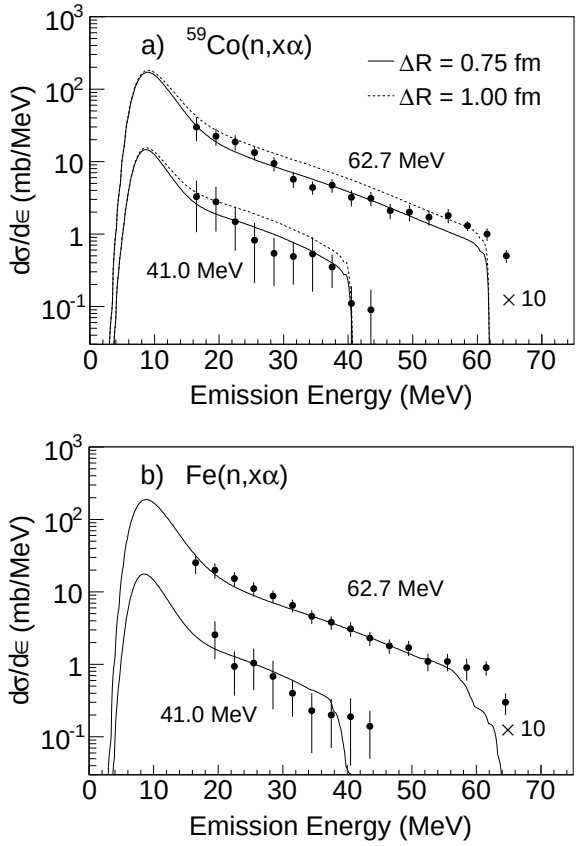

FIG. 4: Angle-integrated $(n, x\alpha)$ spectra for a) ^{59}Co and b) elemental Fe at incident energies of 41.0 and 62.7 MeV. The present calculations are compared with the experimental data of Nica *et al.* [38] for ^{59}Co and Slypen *et al.* [20] for Fe.

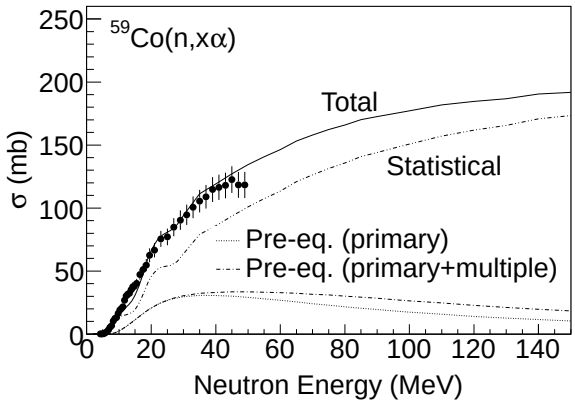

FIG. 5: Calculated $(n, x\alpha)$ cross sections for ^{59}Co which are compared with the experimental data of Grimes *et al.* [10]. The total production cross sections are the sum of those from the multiple pre-equilibrium and the statistical decay processes.

section are rather global predictions with a common set of model parameters.

A. ^{59}Co

The model calculation is compared with the experimental data for ^{59}Co in Fig. 5. The alpha-particle production cross sections were measured at LANSCE up to 50 MeV, and the details of the experiment are reported elsewhere [10]. In this figure, the dotted curve plots only the primary pre-equilibrium cross section (Eq. (3) and (5)), while the dot-dashed curve shows the cross section which includes the multiple process (Eq. (3), (5) and Eq. (7)). Our calculated total alpha-production cross sections reproduce the experimental data very well. As the incident energy increases, the statistical decay cross section becomes much larger than the pre-equilibrium process as plotted by the dot-dot-dashed curve, because more channels that produce alpha-particles open up. Nevertheless, the pre-equilibrium process is still important above 10 MeV to give the total alpha-particle production cross sections that are consistent with the experimental data. It should be noted that the pre-equilibrium component reaches about 35% of the total amount in the energy range from 15 to 30 MeV. The pre-equilibrium emission reaches a maximum at about 30 MeV, and it then decreases gradually. The decreasing tendency mainly comes from the total reaction cross section decreases with neutron energy, as given in Eq. (3), although the other model parameters may give similar energy dependencies.

The calculated total alpha-particle production cross section increases rapidly near the threshold energy, and the slope becomes rather gentle above 50 MeV where no experimental data are available. The extrapolated cross sections above 50 MeV were validated against the experimental data of Fe and Cr, which will be shown later. In the high energy region, the nuclear structure effect becomes less important, hence we expect that the alpha-particle production cross sections for all structural materials may exhibit a similar tendency.

At higher energies, the largest contribution to the total alpha-particle production is from the statistical decay stage, which does not imply that the pre-equilibrium process is just a correction. The alpha-particles emitted during the pre-equilibrium stage remove some amount of the total excitation energy, results in changes in the statistical emission of all particles.

Our calculation reproduces not only the total alpha-particle production cross sections but also the available experimental data for the other reaction channels simultaneously, without any individual tuning to these cross sections. Figure 6 shows the calculated cross sections for the (n, n'), $(n, 2n)$, (n, α) and $(n, n\alpha)$ reactions from

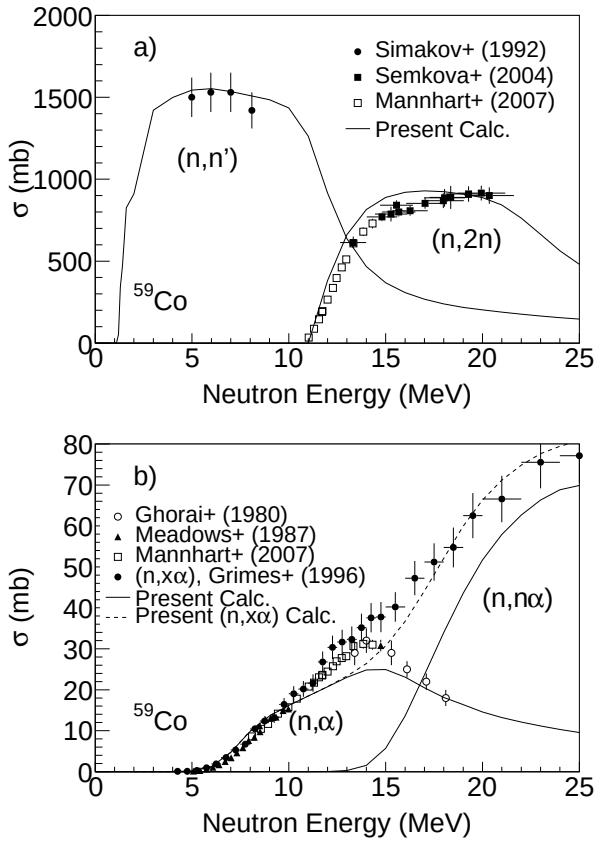

FIG. 6: Present calculations of a) (n, n'), $(n, 2n)$ and b) (n, α), $(n, n\alpha)$ cross sections for ^{59}Co from threshold energies to 25 MeV which are compared with the experimental data taken from the other works [39–41]

their threshold energies to 25 MeV, compared with the experimental data [39–41]. Some of the experimental data shown in Fig. 6 were obtained with the activation method, which we often believe to be reliable. In general, the neutron emission channel, such as the (n, n') and $(n, 2n)$ reactions, has the largest fraction in the total reaction cross section σ_{cn}, while the charged particle emission channels are suppressed by the Coulomb barrier. Our calculated cross sections reproduce these experimental data at the same time, as well as the total alpha-particle production cross sections, which suggests that our nuclear reaction modeling and all the model parameters involved are reasonable for neutron reactions on ^{59}Co and on neighboring nuclei.

B. ^{58,60}Ni

Figure 7 shows the alpha-particle production cross sections for ^{58}Ni and ^{60}Ni. The dashed curves show the evaluated cross sections in ENDF/B-VII.0 [9]. The fraction of the pre-equilibrium emission is similar to the case of ^{59}Co — it is smaller than the statistical decay cross sections, but it still has an important contribution to the total alpha-particle emission. Generally, agreement between the calculated excitation functions and the experimental data is reasonable in both isotope cases. An apparent underestimation can be seen in Fig. 7-a) where the calculation tends to be out of the range of experimental uncertainties around 15 MeV for ^{58}Ni. It is not difficult to adjust our calculations to the experimental data by modifying the level density parameters in the statistical decay process, as they have relatively large uncertainties that are shown in Fig. 2. Nevertheless, the comparisons in Fig. 7 provide important information on our prediction capabilities including uncertainties in the calculated cross sections.

To understand the reason of the underestimation in ^{58}Ni$(n, x\alpha)$ — a bump near 15 MeV — we looked into different reaction channels that produce alpha-particles, *i.e.,* (n, α), $(n, n\alpha)$ and $(n, p\alpha)$. The calculated cross sections are compared with the available experimental data [42, 43] from the threshold energies up to 25 MeV in Fig. 8. The (n, α) cross section starts decreasing at 10 MeV where the $(n, n\alpha)$ channel opens. However, the $(n, n\alpha)$ cross section does not rise so steeply that our calculated total alpha-particle production cross section gives the bump shape near 15 MeV. Below 15 MeV, the total alpha-particle production is equivalent to (n, α), but our calculation is already lower than the experimental data of Fessler and Qaim [42], and data from LANSCE. This underestimation in (n, α) can be partly resolved by increasing the asymptotic level density parameter a^* of ^{55}Fe by only 3%, which is shown by the dotted lines in Fig. 8. It also increases the $(n, n\alpha)$ and $(n, p\alpha)$ cross sections, which gives more reasonable $(n, x\alpha)$ cross sections above $\sim$ 15 MeV. The same adjustment might be possible if we decrease the level density parameter of ^{58}Ni. A comprehensive data fitting, which is not a scope of this paper though, can be achieved by adjusting all level density parameters simultaneously.

C. Elemental Cr and Fe

Figure 9 illustrates the cross sections for elemental Cr and Fe. The dashed curves show the evaluated cross sections in ENDF/B-VII.0 [9]. For the Fe case, the earlier VII.0 evaluation was made by an eye-guide fitting to our experimental data above 20 MeV. Our experimental data are in good agreement with those measured by Matsuyama *et al.* [44] below ∼15 MeV, and consistent with 96 MeV data of Blideanu *et al.* [15] for Fe. We performed the model calculations for all natural isotopes, and summed them up by weighting the natural abundances.

Both the experimental and theoretical excitation functions for these nuclei exhibit a rather flat shape above $\sim$ 50 MeV, and we expect similar shapes in the alpha-

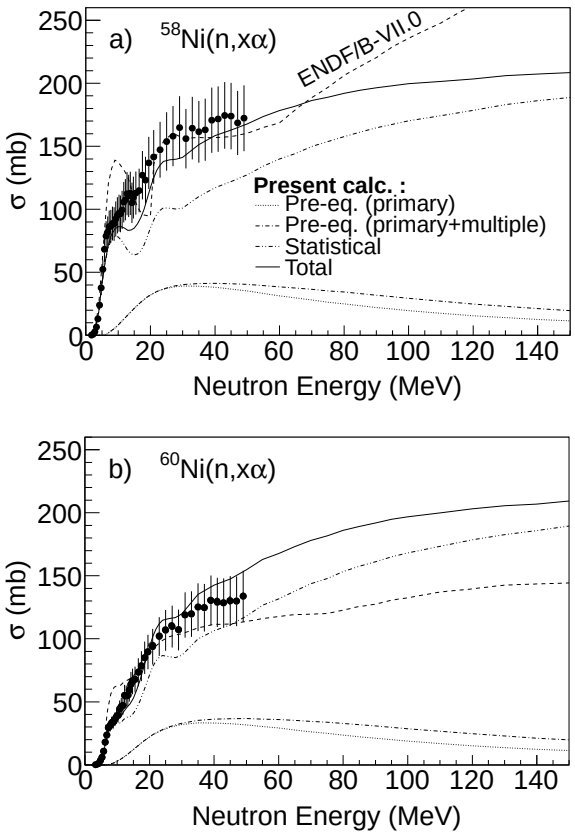

FIG. 7: Calculated $(n, x\alpha)$ cross sections for a) ^{58}Ni and b) ^{60}Ni compared with the experimental data of Haight *et al.* [12]. The total production cross sections are the sum of those from the multiple pre-equilibrium and the statistical decay processes.

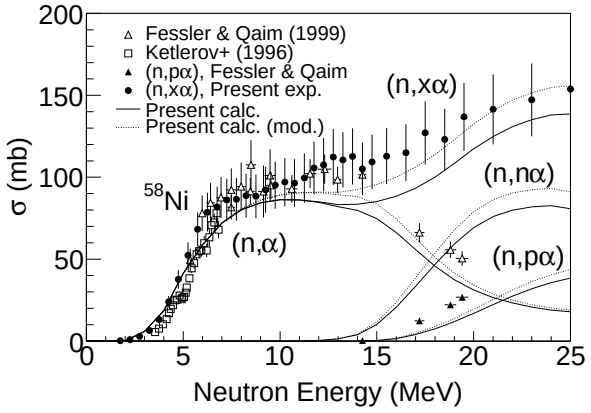

FIG. 8: Present calculations of (n, α), $(n, n\alpha)$, $(n, p\alpha)$ and $(n, x\alpha)$ cross sections for ^{58}Ni from threshold energies to 25 MeV, compared with the experimental data taken from the other works [42, 43]. The dotted curves represent the calculations with 3%-increased asymptotic level density parameter a^* for ^{55}Fe.

particle production cross section for ^{59}Co and ^{58,60}Ni. This gives us some confidence in using our model calculations to extrapolate the alpha-particle production cross sections outside the experimental energy range in Figs. 5 and 7.

For the case of Fe, the calculated cross section agrees fairly well with the experimental data. However, the present calculation largely underestimates the experimental cross sections above 10 MeV for Cr. Note that the pre-equilibrium cross sections are included in this calculation, and give very similar contribution as shown in ^{59}Co and ^{58,60}Ni. If we increase the pre-equilibrium contribution to fit the experimental data, the model parameters will be physically unacceptable. This problem is mainly due to insufficient alpha-particle production in the statistical decay process from ^{52}Cr (83.8% of the natural abundance), as is discussed below.

In Fig. 10, the solid curves show the calculated cross sections for the ^{52}Cr(n, α) and $(n, n\alpha)$ reactions up to 25 MeV. Since there are no other major channels that produce alpha-particles, the underestimation of Cr$(n, x\alpha)$ comes from those reactions. As we carried out a simple sensitivity study of the level density for ^{58}Ni, this underestimation is substantially improved by increasing the asymptotic level density parameter a^* for ^{49}Ti which is the residual nucleus of ^{52}Cr(n, α) reaction. As an example, we calculated reaction cross sections for ^{52}Cr with 10%-increased a^* for ^{49}Ti, and they are shown by the dotted curves in Fig. 10.

Note that the change in the level density parameter, $+0.654$ MeV^{-1}, is within the estimated uncertainty shown in Fig. 2. In addition, this change in the level density does not affect the other channels, because the (n, α) cross sections are much smaller than the others in general. This modification to the level density improves Cr$(n, x\alpha)$ cross sections significantly as illustrated in Fig. 9 by the dotted curve. Although other parameters involved in the decay sequence may change our calculations, the level density parameter of ^{49}Ti has the largest sensitivity to the total alpha-particle production cross sections in this case.

Once the alpha-particle production in the pre-equilibrium process is calculated with the Iwamoto and Harada model, the experimental total alpha-particle production cross sections can be reproduced by relatively small changes in the level density parameters. The Iwamoto and Harada model has one adjustable parameter ΔR, to which we assigned a constant value of 0.75 fm. Through our analysis, it seems we can adopt the same ΔR for different targets in this mass region. Certainly, much attention must be paid to the level density parameters.

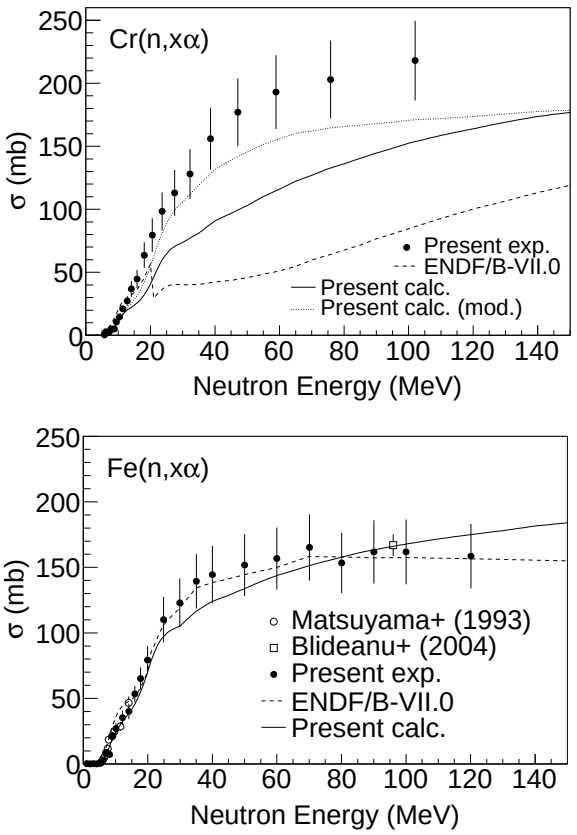

FIG. 9: Calculated $(n, x\alpha)$ cross sections for elemental Cr and Fe which are compared with the present experimental data. The dotted curve in Cr represents the calculation with 10%-increased asymptotic level density parameter a^* for ^{49}Ti.

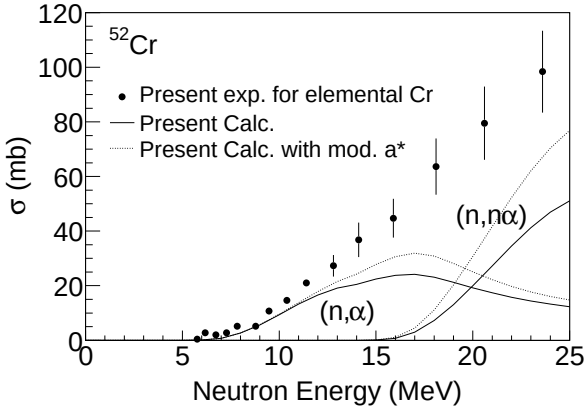

FIG. 10: Calculated (n, α) and $(n, n\alpha)$ cross sections for ^{52}Cr. The dotted curve is calculated by increasing the asymptotic level density parameter a^* for ^{49}Ti by 10%. The present experimental data for elemental Cr are also plotted for the purpose of reference.

V. SUMMARY AND CONCLUSION

We calculated alpha-particle production cross sections with the statistical decay and pre-equilibrium models, with an emphasis on pre-equilibrium cluster emission. The overlap integral in the Iwamoto and Harada clustering model was calculated numerically without the rms approximation. The overall strength of pre-equilibrium emission was determined independently by optimizing the M^2 parameter to fit the experimental (n, xp) pre-equilibrium spectra. Under this condition, we found that a constant ΔR parameter of 0.75 fm, which determines the strength of the alpha-particle emission, gives good agreement with experimental alpha-particle energy spectra over a wide range of incident neutron energy.

Finally, we compared our model calculations with the LANSCE experimental data for ^{59}Co, ^{58,60}Ni, Cr and Fe. The pre-equilibrium contribution to the alpha-particle production is about 30% at about 30 MeV and it decreases monotonically. Our calculated $(n, x\alpha)$ cross sections agree well with the experimental data, except for the Cr case. The statistical decay process exhibits the main contribution to the total alpha-particle production over the whole energy range, and the calculated cross sections are still suffered by uncertainties in the level density parameters. We performed a simple sensitivity study for the level density parameters in combination with a Iwamoto and Harada clustering emission model, and found that relatively small changes in the level density parameters improve the reproduction of experimental data significantly. In reality, there are many options of the level density model and parameters. Some of the useful models and latest parameters are found in Reference Input Parameter Library (RIPL-3) [45], and they may improve the situation.

Acknowledgments

One of the authors (S. K.) thanks Los Alamos National Laboratory for the hospitality during his stay. He is also grateful to Dr. S. Okajima of Japan Atomic Energy Agency who encouraged this study. This work benefitted from the use of the LANSCE accelerator facility as was carried out under the auspices of the National Nuclear Security Administration of the U.S. Department of Energy at Los Alamos National Laboratory under Contract No. DE-AC52-06NA25396.

[1] C. Kalbach, Phys. Rev. C **71**, 034606 (2005).
[2] C. Kalbach, Z. Phys. A **283**, 401 (1977).
[3] A. J. Koning and M. C. Duijvestijn, Nucl. Phys. **A744**, 15 (2004).
[4] A. Iwamoto and K. Harada, Phys. Rev. C **26**, 1821 (1982).
[5] S. Kunieda, T. Fukahori, S. Hirayama, and Y. Watanabe, in *Proc. Intern. Conf. Nuclear Data for Science and Technology, Jeju Island, Korea, April 26-30, 2010* (2011), *J. Kor. Phys. Soc.*, 59, 911 (2011).
[6] J. S. Zhang, S. W. Yan, and C. L. Wang, Z. Phys. A **344**, 251 (1993).
[7] P. G. Young, E. D. Arthur, and M. B. Chadwick, "Comprehensive Nuclear Model Calculations: Introduction to the Theory and Use of the GNASH code," Los Alamos National Laboratory Report No. LA-12343-MS (1992).
[8] M. B. Chadwick, P. G. Young, D. C. George, and Y. Watanabe, Phys. Rev. C **50**, 996 (1994).
[9] M. B. Chadwick, P. Oblozinsky, M. Herman, N. M. Greene, R. D. McKnight and D. L. Smith, P. G. Young, R. E. MacFarlane, G. M. Hale, S. C. Frankle and A. C. Kahler, T. Kawano, R. C. Little, D. G. Madland, P. Moller, R. D. Mosteller, P. R. Page, P. Talou, H. Trellue, M. C. White, W. B. Wilson and R. Arcilla, C. L. Dunford, S. F. Mughabghab, B. Pritychenko, D. Rochman, A. A. Sonzogni, C. R. Lubitz, T. H. Trumbull, J. P. Weinman, D. A. Brown, D. E. Cullen, D. P. Heinrichs, D. P. McNabb, H. Derrien, M. E. Dunn, N. M. Larson, L. C. Leal, A. D. Carlson, R. C. Block, J. B. Briggs, E. T. Cheng, H. C. Huria, M. L. Zerkle, K. S. Kozier, A. Courcelle, V. Pronyaev and S. C. van der Marck, Nucl. Data Sheets, **107**, 2931 (2006).
[10] S. M. Grimes, C. E. Brient, F. C. Goeckner, F. B. Bateman, M. B. Chadwick, R. C. Haight, T. M. Lee, S. M. Sterbenz, P. G. Young, O. A. Wasson and H. Vonach, Nucl. Sci. Eng. **124**, 271 (1996).
[11] R. C. Haight, F. B. Bateman, S. M. Sterbenz, M. B. Chadwick, P. G. Young, S. M. Grimes, O. A. Wasson, P. Maier-Komor, and H. Vonach, in *Proc. Intern. Conf. on Nuclear Data for Science and Technology, Trieste, Italy, 1997*, edited by G. Reffo (ENEA, Bologna, Italy, 1997), p. 603.
[12] R. Haight, F. Bateman, S. Sterbenz, S. Grimes, O. Wasson, P. Maier-Komor, and H. Vonach, Fusion Eng. and Design **37**, 73 (1997).
[13] R. C. Haight, in *Proc. Intern. Conf. Nuclear Data for Science and Technology, April 22-27, 2007, Nice, France*, edited by O. Bersillon, F. Gunsing, E. Bauge, R. Jacqmin, and S. Leray (EDP Sciences, 2008), p. 1081.
[14] E. Raeymackers, I. Slypen, S. Benck, J. P. Meulders, N. Nica, and V. Corcalciuc, At. Data Nucl. Data Tables **87**, 231 (2004).
[15] V. Blideanu, F. R. Lecolley, J. F. Lecolley, T. Lefort, N. Marie, A. Atac, G. Ban, B. Bergenwall, J. Blomgren, S. Dangtip, K. Elmgren, Ph. Eudes, Y. Foucher, A. Guertin, F. Haddad, A. Hildebrand, C. Johansson, O. Jonsson, M. Kerveno, T. Kirchner, J. Klug, Ch. Le Brun, C. Lebrun, M. Louvel, P. Nadel-Turonski, L. Nilsson, N. Olsson, S. Pomp, A. V. Prokofiev, P. -U. Renberg, G. Riviere, I. Slypen, L. Stuttge, U. Tippawan and M. Osterlund, Phys. Rev. C, **70**, 014607 (2004).
[16] I. Slypen, V. Corcalciuc, J. P. Meulders, and M. B. Chadwick, Phys. Rev. C **53**, 1309 (1996).
[17] M. B. Chadwick, H. H. Barschall, R. S. Caswell, P. M. DeLuca, G. M. Hale, D. T. Jones, R. E. MacFarlane, J. P. Meulders, H. Schuhmacher, U. J. Schrewe, A. Wambersie and P. G. Young, Medical Physics **26**, 974 (1999).
[18] F. B. Bateman, R. C. Haight, M. B. Chadwick, S. M. Sterbenz, S. M. Grimes, and H. Vonach, Phys. Rev. C **60**, 064609 (1999).
[19] M. B. Chadwick and E. Norman, IEEE Transactions on Nucl. Science **46**, 1386 (1999).
[20] I. Slypen, N. Nica, A. Koning, E. Raeymackers, S. Benck, J. P. Meulders, and V. Corcalciuc, J. Phys. G: Nucl. Part. Phys. **30**, 45 (2004).
[21] R. C. Haight, F. B. Bateman, S. M. Sterbenz, S. M. Grimes, O. A. Wasson, P. Maier-Komor, and H. Vonach (to be published).
[22] E. Beták and J. Dobeš, Z. Phys. A **279**, 319 (1976).
[23] P. Obložinský, Nucl. Phys **A453**, 127 (1986).
[24] F. C. Williams, Nucl. Phys. **A166**, 231 (1971).
[25] C. Kalbach, Phys. Rev. C **32**, 1157 (1985).
[26] L. I. Schiff, "Quantum Mechanics", MacGraw-Hill, New York (1968).
[27] S. Kunieda, S. Chiba, K. Shibata, A. Ichihara, and E. S. Soukhovitskiĭ, J. Nucl. Sci. Technol. **44**, 838 (2007).
[28] E. Sh. Soukhovitskiĭ, S. Chiba, O. Iwamoto, K. Shibata, T. Fukahori, and G. B. Morogovskiĭ, JAERI-Data/Code 2005-002, Japan Atomic Energy Research Institute (2005).
[29] M. Avrigeanu, A. C. Obreja, F. L. Roman, V. Avrigeanu, and W. von Oertzen, At. Data Nucl. Data Tables **95**, 501 (2009).
[30] M. Avrigeanu and V. Avrigeanu, Phys. Rev. C **79**, 027601 (2009).
[31] J. Raynal, in *Proc. of the Specialists' Meeting on the Nucleon Nucleus Optical Model up to 200 MeV, 13-15 November 1996, Bruyères-le-Chatel, France* (OECD/NEA, 1997), pp. 159–166.
[32] A. Gilbert and A. G. W. Cameron, Can. J. Phys. **43**, 1446 (1965).
[33] A. V. Ignatyuk, G. N. Smirenkin, and A. S. Tishin, Sov. J. Nucl. Phys. **21**, 255 (1975).
[34] W. D. Myers and W. J. Swiatecki, Nucl. Phys. **81**, 1 (1966).
[35] S. F. Mughabghab, *Atlas of Neutron Resonances: Thermal Cross Sections, Resonance Parameters* (Elsevier, Amsterdam, 2006).
[36] C. Kalbach, Z. Phys. A **287**, 319 (1978).
[37] C. Kalbach, Phys. Rev. C **69**, 014605 (2004).
[38] N. Nica, S. Benck, E. Raeymackers, I. Slypen, J. P. Meulders, and V. Corcalciuc, J. Phys. G: Nucl. Part. Phys. **28**, 2823 (2002).
[39] W. Mannhart and D. Schmidt, Tech. Rep. PTB-N-53, Physikal. Techn. Bundesanst., Braunschweig (2007).
[40] V. Semkova, V. Avrigeanu, T. Glodariu, A. J. Koning, A. J. M. Plompen, D. L. Smith, and S. Sudár, Nucl. Phys. **A730**, 255 (2004).
[41] S. P. Simakov, G. N. Lovchikova, V. P. Lunev, V. G. Pronyaev, N. N. Titarenko, and A. M. Trufanov, Vop. At. Nauki i Tekhn., Ser. Yadernye Konstanty, Issue 4 p. 74 (1992), (in Russian).

[42] A. Fessler and S. M. Qaim, Radiochim. Acta **84**, 1 (1999).
[43] V. V. Ketlerov, A. A. Goverdovskiy, V. F. Mitrofanov, Y. B. Ostapenko, and V. Y. Khryachkov, Vop. At. Nauki i Tekhn., Ser. Yadernye Konstanty, Issue 1 p. 121 (1996), (in Russian).
[44] I. Matsuyama, M. Baba, S. Matsuyama, T. Kiyosumi, T. Sanami, N. Hirakawa, N. Ito, S. Chiba, T. Fukahori, M. Mizumoto, K. Hasegawa and Sh. Meigo, in *Proc. of the 1993 Symposium on Nuclear Data, Nov. 18-19, 1993, JAERI, Tokai, Japan*, JAERI-M 94-019 (1994), p. 191.
[45] R. Capote, M. Herman, P. Oblozinsky, P. G. Young, S. Goriely, T. Belgya, A. V. Ignatyuk, A. J. Koning, S. Hilaire, V. A. Plujko, M. Avrigeanu, O. Bersillon, M. B. Chadwick, T. Fukahori, Z. Ge, Y. Han, S. Kailas, J. Kopecky, V. M. Maslov, G. Reffo, M. Sin, E. Sh. Soukhovitskii and P. Talou, Nucl. Data Sheets, **110**, 3107 (2009).